Scanning tunnelling microscopic and spectroscopic investigation of the microstructural and electronic properties of the grain boundaries of giant magnetoresistive manganites

1998 J. Phys.: Condens. Matter 10 10795

(http://iopscience.iop.org/0953-8984/10/48/003)

J. Phys.: Condens. Matter **10** (1998) 10795–10804. Printed in the UK PII: S0953-8984(98)93530-5

Scanning tunnelling microscopic and spectroscopic investigation of the microstructural and electronic properties of the grain boundaries of giant magnetoresistive manganites

A K Kar†, A Dhar†, S K Ray†, B K Mathur†, D Bhattacharya‡ and K L Chopra§

† Department of Physics and Meteorology, Indian Institute of Technology, Kharagpur 721 302, India

‡ Materials Science Centre, Indian Institute of Technology, Kharagpur 721 302, India

§ Thin Film Laboratory, Department of Physics, Indian Institute of Technology, New Delhi 110 016, India

Received 22 April 1998, in final form 27 August 1998

Abstract. Scanning tunnelling microscopic (STM) and spectroscopic (STS) investigations have been carried out on the grain boundaries (GBs) of sintered pellets of giant magnetoresistive perovskite manganites $La_{0.67}Ca_{0.33}MnO_3$ (LCMO), $La_{0.60}Y_{0.07}Ca_{0.33}MnO_3$ (LYMCO) and $La_{0.67}Pb_{0.10}Ca_{0.23}MnO_3$ (LPMCO). Based on spectroscopic data obtained and estimation of band gap, it has been concluded that these materials possess some sort of semiconducting intergranular layer (IGL) whose thicknesses are in the range of a few nm to about 100 nm and the band gap is in the range of 0.3–0.45 eV. IGLs are usually more resistive than the grains. For semiconducting samples like LCMO and LYCMO (room temperature band gap $= 0.23$ and 0.27 eV respectively), IGLs bend the energy band near GBs. This bending has been estimated to be about 40–50 meV with the depletion depth of few tens of nm extending on both sides of the IGL. The decrease in conductivity near the GB is due to the disorder induced carrier scattering and the bending of the band. LPCMO is almost conducting at room temperature. The GBs in this material sometimes exhibit conducting behaviour which may be due to the accumulation of some conducting material or the trapping centres in the IGL. Scanning electron microscopic and electrical measurements also justify the STM/STS results.

1. Introduction

Present information and data storage technology demands an enhancement of sensitivity of magnetoresistive reading head material by several times over conventional magnetic material [1, 2]. The discovery of giant magnetoresistance (GMR) in perovskite manganites [3–7] has designated these materials to be potential sensor candidates for reading heads. A number of researchers have studied the effects of microstructural aspects [8–10], grain boundaries [11–16] and artificial magnetic tunnel junctions [17–19] on magnetoresistance. It has been established that a substantial amount of the contribution to MR arises from GBs below the transition temperature and at low field the large MR appears from the spin-polarized tunnelling between grains [20].

The role of the intergranular layer in GMR materials, such as its influence on magnetotunnelling and its function as a weak link isolating intragranular high

0953-8984/98/4810795+10$19.50

magnetoresistive regions, is yet to be established [7]. The present challenge lies in the manipulation of GBs for enhanced MR at low field [12]. Tailoring of a GB requires a detailed study of its physical properties, like its microstructure, electronic nature, composition, magnetic and electrical properties, crystallographic structure etc, which may be responsible for controlling the magnetotransport properties. Scanning tunnelling microscopic (STM) and spectroscopic (STS) investigations have aimed at elucidating the microstructural and electronic properties of the grain boundaries of GMR materials.

2. Experimental details

The powders of perovskite oxides $La_{0.67}Ca_{0.33}MnO_3$, $La_{0.60}Y_{0.07}Ca_{0.33}MnO_3$ and $La_{0.67}Pb_{0.10}Ca_{0.23}MnO_3$ were synthesized following a flash pyrophoric process [21]. Aqueous solutions of nitrate salts of the cations were mixed in a beaker in appropriate ratio and glycine was added to it so that the total amount of cations in the mixture and the amount of glycine was in the ratio 1:5. A mixture of an aqueous solution containing polyvinyl alcohol, polyacrylonitrile and polyacrylamide was added to the above mixture and the beaker was placed in a pit type furnace preheated to 350 °C. The solution first dried up to form a gel which then explosively decomposed to yield very fine powder. The powders were pelletized and sintered at 1400 °C for five hours in air. Only for lead samples the sintering temperature was 1100 °C.

The resistivity measurements of these samples with variation of temperature were conducted by a conventional four probe method using a closed cycle He refrigerator (APD Cryogenics, HC-2, USA). A magnetic field of 3.5 kG was used to measure magnetoresistance. Crystalline homogeneity was tested by a scanning electron microscope (SEM) (JEOL Scanning Microscope, JSM-5200, Japan).

Before STM/STS study, the samples were baked at about 300 °C to remove adsorbed moisture for topographic and spectroscopic investigations. Fresh surface was obtained by breaking the pellet and it was then mounted on STM stubs using silver paint. The surface was studied by a commercial STM (model UHV-635 of RHK Technology, Inc., USA) in air at room temperature using electrochemically etched tungsten tips. In tunnelling spectroscopy (TS), the voltage dependence of tunnelling current was studied locally at constant tip–sample separation. In all the samples tunnelling spectra were acquired by freezing the tip position corresponding to a tunnelling current of 100 pA and a tip–sample separation voltage of 0.4 V. A separation voltage corresponds to a particular tip to sample distance. The current–voltage (I–V) data were obtained with feedback loop interrupted by the sample and hold circuit [22, 23]. The signal was averaged over ten spectra at each sample point. Sample sites were chosen on the grain, near the GB and on the GB. To explore the grain boundary properties, a series of I–V spectra was taken along and across the boundaries. Reproducibility was checked by acquiring data at different locations and at different tip to sample distances.

3. Results and discussion

The resistivity of these materials passes a critical temperature which corresponds to a metal–semiconductor transition temperature (T_{ms}). Above this temperature the material shows semiconducting behaviour, below it, this has metallic character (figure 1). T_{ms} for LCMO, LYCMO and LPCMO are 268 K, 176 K and 300 K respectively. The Curie temperatures (T_c) of the specimens have been measured to be at 235 K, 171 K and 304 K respectively. These are in fair agreement with reported values [15, 24–29].

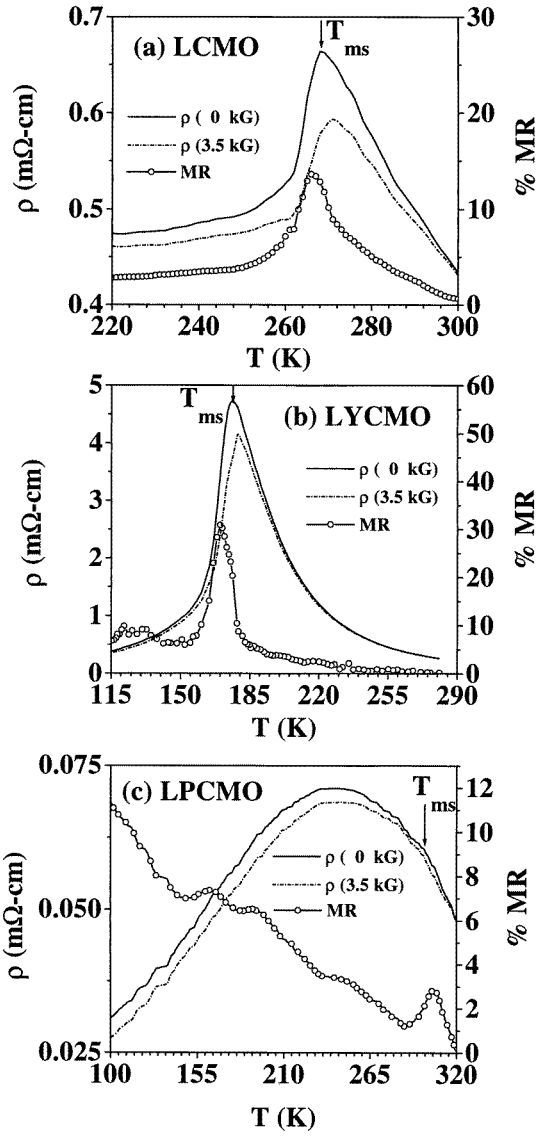

Figure 1. The temperature dependence of resistivity in zero and 3.5 kG magnetic field and the GMR ratio, defined as $[\rho(0) - \rho(H)]/\rho(0)$, of (a) LCMO, (b) LYCMO and (c) LPCMO. The metal–semiconductor transition temperature (T_{ms}) is indicated by an arrow.

Surfaces of the samples were found to be stable and unchanged in air even after two hours of cleaving. A gradual surface degradation has been noticed on prolonged exposure to air giving arbitrary and obscure surface features, indicating the presence and formation of some sort of insulating or semiconducting layer. All these sintered ceramics possess the same overall microstructures. Figure 2 represents two such SEM micrographs of different magnifications. The microstructural features indicate real crystalline homogeneity of the material with the presence of distinct grain boundaries and absence of cavities or voids.

Grain size varies from about 1 micron to few microns. Primary topograhic features observed in STM studies are the presence of large grains (several μm in dimension) which is in good agreement with SEM micrographs, and almost straight terraces of varying lengths (100–1000 nm). Crystallographic facets of broken surfaces of these materials appear to be terraces of integer or half integer multiples of unit cell height.

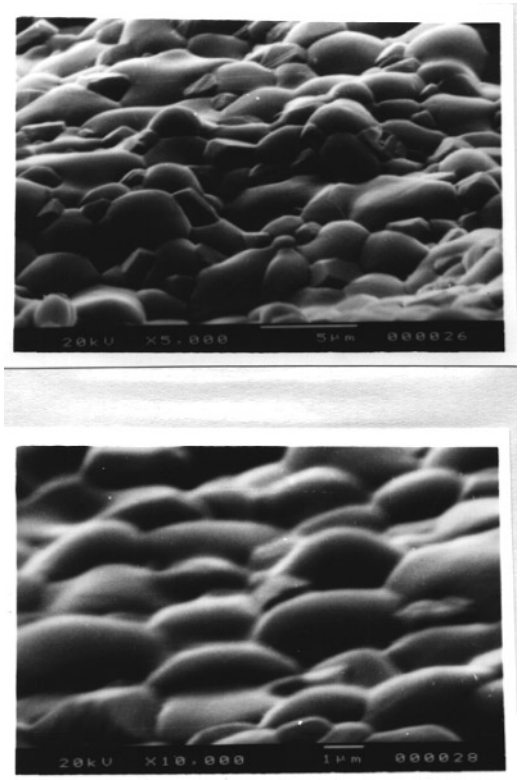

Figure 2. Two representative SEM micrographs of the specimens, indicating granular homogeneous crystalline microstructures of the materials.

The STM features are not just the geometrical attribute of the surface, they are mainly dependent on the electronic structure of this surface. This furnishes the constant density of states (DOS) profile in the topographic or constant current mode. Local variation of the electronic nature creates different morphological impressions [30]. Observed traits are exclusively geometric ones only when the surface is electronically homogeneous. Inhomogeneity in the electronic nature of the surface portrays a combination of the two. In such a case it is very difficult to interpret the images, which is where tunnelling spectroscopy comes into play. From the nature of the I–V data one can conclude whether a region is electronically homogeneous or not, i.e. whether the region is locally conducting, semiconducting or insulating. Based on combined morphological and spectroscopic studies, it is inferred that some depressed surface morphological features in these materials correspond to regions of comparatively increased resistivity. These regions are likely to be grain boundaries.

Figure 3 displays few typical GBs of these materials taken in constant current mode. Figure 3(a) is a picture of LPCMO which shows sharp and very narrow GBs. Figure 3(b)

shows a wide GB of LYCMO, identified from the image contrast arising from the variation of local electronic nature of the material surface. The depressed canal-like region in figure 3(b), represented by the darker shades of grey, running almost parallel to the top and bottom of this figure is a low conductivity region. Therefore, it may be considered to be a GB intergranular layer, which may not necessarily be a geometrical crevice. Figure 3(c) presents GBs of relatively narrow width of LCMO. A junction of three grains of LCMO is shown in figure 3(d). The width of GBs has been noticed to vary from a few nm to about 100 nm.

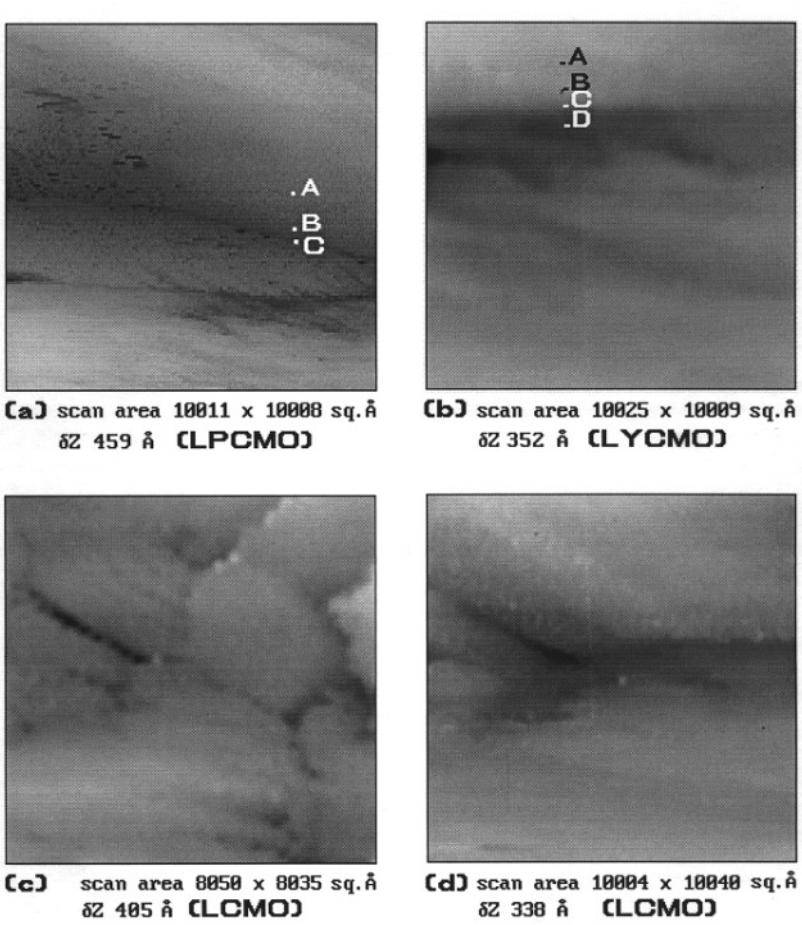

Figure 3. STM topographs of few typical grain boundaries found in these materials: (a) two sharp GBs, (b) a wider GB with thicker IGL deduced from tunnelling spectroscopy, (c) a few narrower GBs, (d) a junction of three grains. δz denotes black to white grey scale height variation of the surface.

Figure 4 shows the nature of current–voltage characteristics (left column) with their corresponding DOSs (right column) acquired at and near the GBs of LPCMO (sites C, B and A of figure 3(a)). These diagrams exhibit a gradual change in conductivity as one moves from site A to site C. Sites on the grain and near the grain boundaries (like A and B) are almost conducting in nature with essentially no band gap, while sites at the grain boundary (like C) are semiconducting with a distinct energy gap ($\sim$0.32 eV) near the Fermi level (E_F). The Fermi level at most of the grain boundaries is near the mid-point between

the valence band edge (E_V) and conduction band edge (E_C) and so it can be said that the semiconducting region does not deviate much from the intrinsic type. In this topograph, though the IGL is not visible, it has a width of a few nm. Other GBs with relatively large widths of IGL also show similar behaviour. Resistivity at points close to the grain boundaries (like sites B) is larger than that at sites on the grain. This increase in resistivity can be attributed to the disorder induced carrier scattering at the interface. Here the low conductivity sites have been found to extend in the regions less than 30 nm on both sides of GB.

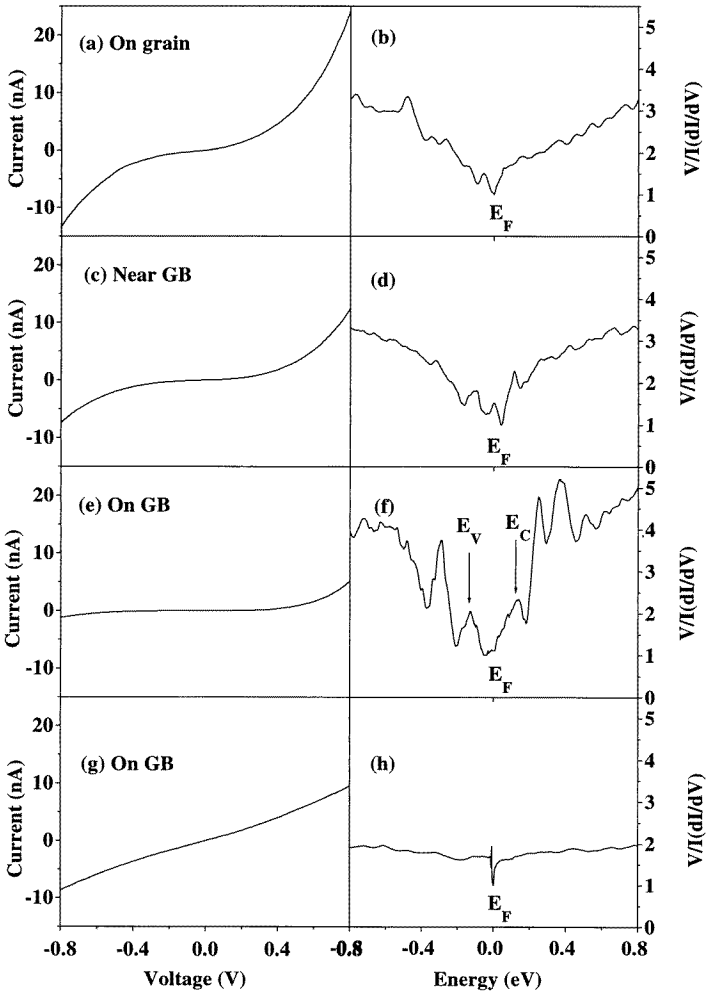

Figure 4. Site specific tunnelling spectroscopic I–V characteristics and corresponding DOS structures of LPCMO (figure 3(a)): (a), (b) on the grain at site A, (c), (d) near the GB at B, (e), (f) on the GB at C and (g), (h) on some particular sites along the GB.

An anomaly in the behaviour of these IGLs has also been distinguished. At certain locations on the grain boundaries, the behaviour is absolutely metallic as shown in figure 4(g) and (h). The DOS near E_F in this case is almost flat compared to those seen at other

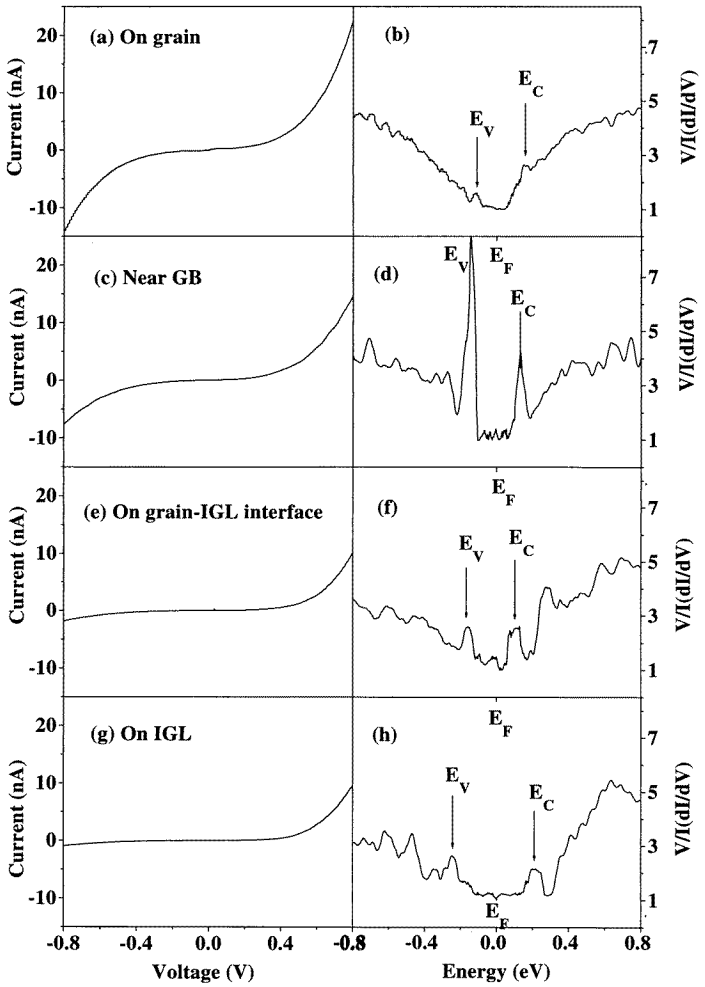

Figure 5. Site specific tunnelling spectroscopic I–V characteristics and corresponding DOS structures of LYCMO (figure 3(b)): (a), (b) on the grain at site A, (c), (d) near the GB at B, (e), (f) on the grain–IGL interface at C and (g), (h) on the IGL at D.

locations where the behaviour is semiconducting. It may be a metallic GB precipitation or cluster formation or some sort of conducting oxide. There may also exist trapped charge carriers in the defect sites along the GB.

The current–voltage characteristics (left) with their corresponding density of states (right), acquired at different sites on an LYCMO sample (topograph in figure 3(b)), are shown in figure 5. Sites on the grain (such as site A) are semiconducting having a gap of about 0.27 eV. The position of E_F suggests that the material is p type. As one approaches the grain boundary (to points such as site B), the band gap remains nearly same, but the E_F shifts slightly towards the conduction band. At the interface of the grain and IGL (at points such as site C), the behaviour is rectifying with E_F shifted towards E_C (figure 5(e) and (f)). The TS (figure 5(g)), acquired at the middle of the shaded region (site D), which is considered to be an IGL, shows wider gap ($\sim$0.43 eV). A gradual decrease in conductivity

is significant in the above sequence of observations. Here the contribution to the resistance originates from both space charge and structural disorder. Gradual shift in E_F implies band bending due to space charge accumulation along the GB interface, estimates to be about 40–50 meV (figure 6). The band bending extends over a width of a few tens of nanometres at the grain boundary. The existence of in-gap surface states on the IGL and on the grain–IGL interface is evident from figures 5(f) and 5(h). Such in-gap surface states have also been found at many locations on the grains and near the grain boundaries. The GBs of LCMO exhibit very similar behaviour as in LYCMO with slightly reduced gap value.

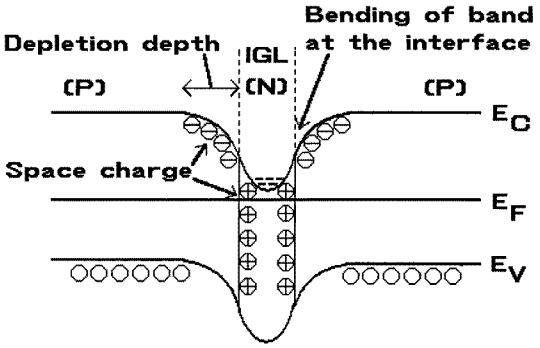

Figure 6. A simplified energy band diagram of a GB with IGL having semiconducting nature.

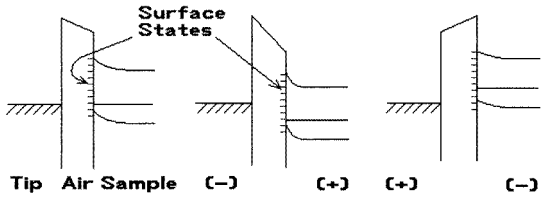

Figure 7. The energy band diagram of STM tip–sample interaction showing metal–insulator–semiconductor junction (tip–air–sample) with the existence of surface states.

The energy gap value of IGL in these materials has been observed to vary in a range of values. This may be due to the local change in composition along GB. The local electronic nature (whether p type or n type) could be decided from the impurity states in the gap. But they could not be resolved properly, possibly due to the existence of surface states. The electronic structure near E_F in these materials may not be of rigid band type [31]. This may be one reason for the appearance of various unidentified peaks in the DOS structures. It is also possible that energy levels can exist inside the gap [32]. Existence of in-gap surface states can never be neglected specially while working in air [33]. The asymmetry exhibited by the tunnelling I–V data arises from a number of factors like local metal–insulator–semiconductor/metal (tip–air–sample) band structure [32], capacitive effect between tip and sample surface, existence of surface states etc, making the process very complex. It can be noticed that the STS properties on the grains do not anyway deviate from the transport properties shown in figure 1(a), (b) and (c).

To understand the increase in resistance across a GB its energy band diagram has been depicted in figure 6. For simplicity it has been assumed that the energy gap of both the crystal and IGL material are the same and the work function of the crystal is less than that of the IGL. The bulk has been assumed to be p type and the IGL to be an n-type semiconductor. So, the interface of a grain and the IGL being a p–n junction, GBs form p–n–p junctions. Creation of space charge at the interface bends the band at each interface producing a well at the IGL. The depth of the depletion layer due to the space charge has also been shown, which in these samples has been measured to be a few tens of nm and found to extend on both sides of the GB. The electrons accumulated at this well requires more energy to overcome the barrier, enhancing resistivity near the interface. The nature of this well depends on the electronic nature of the IGL. Accordingly it may act like a barrier or a well. Whatever may be the electronic nature of the material (metal, semiconductor or insulator) in between the grains, it always forms some sort of barrier to the carrier conduction increasing resistance at the GB. Eventually if it is a metal its topographic signature may not exist, because the metallic material at this point is in a potential well as is the case for figure 5(g), (h).

In an STM the probe tip is a metal, the air acts as an insulating barrier and the sample here can be assumed either a semiconductor or a metal, creating a metal–insulator–semiconductor structure, as shown in figure 7. The electrons tunnel this insulating air barrier. The nature of the I–V characteristics will depend on the site specific electronic band structure of the sample. Consequently the electrons being tunnelled at the GB or near the GB are also expected to face the resistance due to the well, producing a poorly conductive nature of I–V. The existence of surface states facilitates the carrier conduction.

4. Conclusion

STM/STS investigation of the broken surfaces of sintered pellets of GMR oxides LCMO, LYCMO and LPCMO demonstrates that these are fairly stable even after two hours of exposure in air. Morphological study shows a quite granular nature of the crystal surface with crystal facets. Grain boundaries are found to possess IGLs of varying thickness having different electronic nature. TS study exhibits that it is semiconducting and n type in nature in LYCMO and LCMO while the bulk crystal appeared to be p type. In LPCMO it is also semiconducting. LPCMO is metallic at room temperature. IGLs are found to be more resistive with higher band gap value than the crystallite sites. Its band gaps are found to vary between 0.3 and 0.45 eV. LCMO and LYCMO crystal gap values are about 0.23 and 0.27 eV respectively. Their GBs have space charge regions of depletion depth of few tens of nm. The increase in resistivity in this case appears to be due to the space charge and crystallographic disorder. The band bends at the interface due to the creation of space charge which increases GB resistance. The band bending has been measured to be about 40–50 meV. It has been often found to show metallic behaviour indicating the existence of some sort of metallic phase. The possibility of trapped charge carriers in defect sites also cannot be ignored. These local anisotropies can influence the magnetotransport properties.

Acknowledgment

One of the authors, AKK, acknowledges the financial support of the Council of Scientific and Industrial Research, HRDG, India, provided during the research.

References

[1] Brng J A, Tran L, Bhattacharyya M, Nickel J H, Anthony T C and Jander A 1996 *J. Appl. Phys.* **79** 4491
[2] Mallinson J C 1996 *Magneto-Resistive Heads: Fundamentals and Applications* (San Diego, CA: Academic)
[3] von Helmholt R, Wecker J, Holszapfel B, Schultz L and Samwer K 1993 *Phys. Rev. Lett.* **71** 2331
[4] Chahara K-I, Toshiyuki O, Masahiro K and Yuzoo K 1993 *Appl. Phys. Lett.* **63** 1990
[5] Jin S, McCormack M, Tiefel T H and Ramesh R 1994 *J. Appl. Phys.* **76** 6929
[6] Jin S, Tiefel T H, McCormack M, Fastnacht R A, Ramesh R and Chen L H 1994 *Science* **264** 413
[7] McCormack M, Jin S, Tiefel T H, Fleming R M, Phillips J M and Ramesh R 1994 *Appl. Phys. Lett.* **64** 3045
[8] Yeh N-C, Fu C-C, Wei J Y T, Vasquez R P, Huynh J, Maurer S M, Beach G and Beam D A 1997 *J. Appl. Phys.* **81** 5499
[9] Gommert E, Cerva H, Rucki A, Helmolt R V, Wecker J, Kuhrt C and Samwer K 1997 *J. Appl. Phys.* **81** 5496
[10] Wilson M L, Byers J M, Dorsey P C, Horwitz J S, Chrisey D B and Osofsky M S 1997 *J. Appl. Phys.* **81** 4971
[11] Mathur N D, Burnell G, Isaac S P, Jackson T J, Teo B-S, MacManus-Driscoll J L, Cohen L F, Evetts J E and Blamire M G 1997 *Nature* **387** 266
[12] Gupta A, Gong G Q, Xiao Gang, Duncombe P R, Lecoeur P, Trouilloud P, Wang Y Y, Dravid V P and Sun J Z 1996 *Phys. Rev.* B **54** R15 269
[13] Krishnan Kannan M, Modak A R, Lucas C A, Michel R and Cherry H B 1996 *J. Appl. Phys.* **79** 5169
[14] Mahesh R, Mehandiran R, Raychaudhuri A K and Rao C N R 1996 *Appl. Phys. Lett.* **68** 2291
[15] Ju H L and Sohn Hyunchul 1997 *Solid State Commun.* **102** 463
[16] Jia Y X, Lu Li, Khazeni K, Crespi V H, Zettl A and Cohen M L 1995 *Phys. Rev.* B **52** 9147
[17] Lu Yu, Li X W, Gong G Q, Xiao Gang, Gupta A, Lecouer P, Sun J Z, Wang Y Y and Dravid V P 1996 *Phys. Rev.* B **54** R8357
[18] Li X W, Lu Yu, Gong G Q, Xiao Gang, Gupta A, Lecouer P, Sun J Z, Wang Y Y and Dravid V P 1997 *J. Appl. Phys.* **81** 5509
[19] Sun J Z, Krusin-Elbaum L, Duncombe P R, Gupta A and Laibowitz R B 1997 *Appl. Phys. Lett.* **70** 1769
[20] Hwang H Y, Cheong S-W, Ong N P and Batlogg B 1996 *Phys. Rev. Lett.* **77** 2041
[21] Bhattacharya D, Pathak L C, Mishra S K, Sen D and Chopra K L 1990 *Appl. Phys. Lett.* **57** 2145
[22] Güntherodt H-J and Wiesendanger R (eds) 1994 *Scanning Tunneling Microscopy I: General Principles and Applications to Clean and Adsorbate-Covered Surfaces* (Berlin: Springer)
[23] Wiesendanger R 1994 *Scanning Probe Microscopy and Spectroscopy, Methods and Applications* (Cambridge: Cambridge University Press)
[24] Mahendiran R, Mahesh R, Raychaudhuri A K and Rao C N R 1995 *Solid State Commun.* **94** 515
[25] Schiffer P, Ramirez A P, Bao W and Cheong S-W 1995 *Phys. Rev. Lett.* **75** 3336
[26] Li Zisen, Zeng X T and Wong H K 1996 *J. Appl. Phys.* **79** 5188
[27] Fontcuberta J, Martínez B, Seffar A, Piñol S, García-Muñoz J L and Obradors X 1996 *Phys. Rev. Lett.* **76** 1122
[28] De Teresa J M, Blasco J, Ibarra M R, García J, Marquina C, Algarabel P and del Moral A 1996 *J. Appl. Phys.* **79** 5175
[29] Liu J Z, Chang I C, Irons S, Klavins P and Shelton R N 1995 *Appl. Phys. Lett.* **66** 3218
[30] Rohrer G S and Bonnell D A 1990 *J. Am. Ceram. Soc.* **73** 3026
[31] Saitoh T, Bocquet A E, Mizokawa T, Namatame H, Fujimori A, Abbate M, Takeda Y and Takano M 1995 *Phys. Rev.* B **51** 13 942
[32] Bonnell D A and Clarke D R 1988 *J. Am. Ceram. Soc.* **71** 629
[33] Davydov D N, Mayou D, Berger C, Gignoux C, Neumann A, Jansen A G M and Wyder P 1996 *Phys. Rev. Lett.* **77** 3173